

# Nonlinear standing waves in an array of coherently coupled Bose-Einstein condensates

Christian Baals,<sup>1,2</sup> Herwig Ott,<sup>1</sup> Joachim Brand,<sup>3</sup> and Antonio Muñoz Mateo<sup>3</sup>

<sup>1</sup>*Department of Physics and Research Center OPTIMAS,*

*Technische Universität Kaiserslautern, 67663 Kaiserslautern, Germany*

<sup>2</sup>*Graduate School Materials Science in Mainz, Staudinger Weg 9, 55128 Mainz, Germany*

<sup>3</sup>*Dodd-Walls Centre for Photonic and Quantum Technologies,*

*Centre for Theoretical Chemistry and Physics, New Zealand Institute for Advanced Study,*

*Massey University, Private Bag 102904 NSMC, Auckland 0745, New Zealand*

(Dated: June 27, 2018)

Stationary solitary waves are studied in an array of  $M$  linearly-coupled one-dimensional Bose-Einstein condensates (BECs) by means of the Gross-Pitaevskii equation. Solitary wave solutions with the character of overlapping dark solitons, Josephson vortex – antivortex arrays, and arrays of half-dark solitons are constructed for  $M > 2$  from known solutions for two coupled BECs. Additional solutions resembling vortex dipoles and rarefaction pulses are found numerically. Stability analysis of the solitary waves reveals that overlapping dark solitons can become unstable and susceptible to decay into arrays of Josephson vortices. The Josephson vortex arrays have mixed stability but for all parameters we find at least one stationary solitary wave configuration that is dynamically stable. The different families of nonlinear standing waves bifurcate from one another. In particular we demonstrate that Josephson-vortex arrays bifurcate from dark soliton solutions at instability thresholds. The stability thresholds for dark soliton and Josephson-vortex type solutions are provided, suggesting the feasibility of realization with optical lattice experiments.

## I. INTRODUCTION

The Josephson effect is a prominent manifestation of a macroscopic quantum phenomenon. Since its prediction in the 1960s, it has been thoroughly studied in superconducting systems, and has found plenty of applications in electronic devices [1]. The effect relies on the existence of a complex order parameter describing the dynamics of an underlying Bose condensate of Cooper pairs, and due to this fact the associated phenomenology was soon foreseen and later observed in superfluid helium [2–4]. More recently, the advent of Bose-Einstein condensates (BECs) of ultracold gases has opened many new possibilities for the realization of the Josephson effect. The Josephson equations for the modulus and relative phase of the order parameter, accounting for the superfluid particle number density and the superfluid velocity, respectively, predict a non-dissipative flow across a barrier separating two superfluids. Such a flow has been monitored in experimental realizations by direct observation of the particle current versus chemical potential [5–7], or even the phase-current relationship [8]. These fundamental developments are also promising steps for advances in the emerging field of atomtronics [9].

Most of the research about the Josephson effect in ultracold gases has addressed the case of pointlike junctions, based on the study case of a BEC in a double well potential [10]. Long Josephson junctions that allow for a varying phase along the junction between BECs [11] have comparatively received much less attention, in spite of the fact that these systems can support a very interesting topological structure: the Josephson vortex, or fluxon [1]. These topological objects involve localized supercurrents and have found technical application in the field of superconductors, e.g. they could be used as infor-

mation carrying computational bits, or even qubits, due to the fact that they can trap magnetic flux [12, 13]. In BECs, evidence for spontaneously formed Josephson vortices in linearly coupled one-dimensional BECs during a rapid cooling procedure has only been reported very recently [14] (where they were identified as “sine-Gordon solitons”) after such a mechanism had been proposed theoretically [15].

Theoretical studies on Josephson vortices in BECs have mainly considered systems with two linearly coupled 1D condensates [11, 16–18], and a one-dimensional spinor BEC with internal Josephson effect [19, 20]. The models used to describe coupled 1D BECs start from two linearly coupled Gross-Pitaevskii equations (GPEs) [11], or a coupled Luttinger-liquid model [21]. In the small coupling limit, a sine-Gordon model for the relative phase of the two condensates can be derived where the Josephson vortex becomes a sine-Gordon soliton [11, 21, 22]. Recently the full dispersion relation of moving Josephson vortices and related solitary excitations in the more general coupled Gross-Pitaevskii model has been found [22]. Closely related oscillon excitations, which can be understood as long-lived bound states of Josephson vortices were described in Ref. [23]. Generalizations to tunnel-coupled spinor gases [24], and multidimensional Bose gases [25] have also been considered. But there is an interesting system that has not yet been explored, namely the appearance of Josephson vortices in an array of more than two BECs. Such an arrangement could result from slicing a BEC with an optical lattice in the tight binding regime. The arrangement is analogous to layered superconductors [26] where Josephson junctions between layers are coupled, but the theoretical model used for coupled Josephson junctions in superconductors [27] differs from the coupled Gross-Pitaevskii model used to describe ar-

rays of coupled BECs.

In this paper, we study patterns of Josephson vortices and related solitary waves in arrays of linearly coupled 1D BECs. The whole arrangement forms a discrete version of a single two-dimensional (2D) BEC that could be experimentally realized by subjecting a 2D BEC to a 1D optical lattice in the tight binding regime. Our starting point is the analytical solution of an array of identical, static dark solitons in the 1D BECs. A dark soliton in a single 1D BEC is a well known, stable nonlinear wave. The linear coupling in an array of condensates breaks this condition and can eventually lead to the decay of the solitons. As we will show, however, the stability is (maybe counter-intuitively) preserved for high values of the coupling, whereas the decay into Josephson vortices takes place at low coupling. We characterize a number of possible stationary solitary-wave solutions along with their stability and classify their character in terms of Josephson vortices, solitons, and half-solitons by means of a symbolic representation. Although not all possible stationary solitary waves are stable, there is at least one stable configuration that may remain as a final result of decay processes of unstable solitary waves. We also find situations of multi-stability, where several stable solitary-wave solutions coexist.

The situation of extended dark soliton and Josephson vortex excitations in a stack of coupled 1D BECs is closely related to dark soliton stripes (or planar dark solitons) in 2D or 3D BECs. The snaking instability of the dark soliton, which leads to decay into vortex structures, was observed in BECs [28] and superfluid Fermi gases [29] and studied theoretically in Refs. [30–33]. In close analogy to the results reported in this work, the instability thresholds give rise to bifurcations of symmetry-breaking vortex-type solutions [32, 34–36], of which a single vortex line, also called solitonic vortex, is the only dynamically stable nonlinear wave [32, 37].

This paper is organized in the following way: Section II starts with introducing the model (Sec. II A) and overlapping dark soliton solutions (Sec. II B). After discussing the solitary-wave solutions known for two coupled BECs in Sec. II C, solutions for arrays with an even number of BECs are constructed from the known solutions for two BECs in Sec. II D, and more general solutions are briefly discussed in Sec. II E. Linear stability analysis of the stationary solutions is performed in Sec. III for a ring configuration of coupled BECs, where analytic results for stability thresholds of the dark soliton stack are discussed as well as numerically obtained spectra of unstable modes. The bifurcation scenario of Josephson vortex solutions is discussed in Sec. IV before concluding with a discussion of possible experimental realizations in Sec. V.

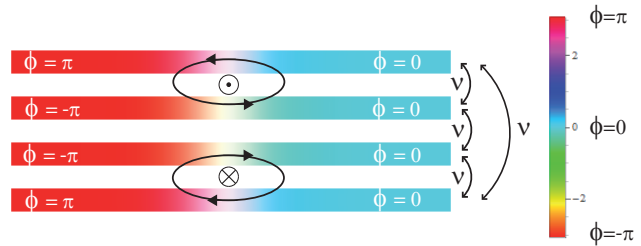


FIG. 1. Schematic of an array with  $M = 4$  coupled 1D BECs described by Eq. (1) with linear coupling  $\nu$  effective between neighboring BECs in the ring configuration (the planar configuration has an identical solution). Shown is a stationary solitary-wave solution in the symmetric Josephson vortex – anti-vortex configuration  $a^*$ . The color encodes the complex phase (per color bar on right) and contrast encodes density. From the phase gradients (differences) encoding superfluid currents (Josephson currents) it can be deduced that the configuration contains one Josephson vortex and one anti-vortex, as indicated. Symbolically, we represent the configuration by  $\downarrow \odot \uparrow \otimes \downarrow$ .

## II. SYSTEM: STACK OF BECS

### A. Gross-Pitaevskii model

Consider an array of  $M$  one dimensional BECs with linear coherent tunnel coupling between nearest neighbors arranged as shown in Fig. 1. Both the ring (periodic) and planar (open) configurations of the array can be modeled by wave functions  $\Psi_j(x, t)$  with  $j = 1, 2, \dots, M$ , satisfying the coupled GPEs

$$i\hbar \frac{\partial \Psi_j}{\partial t} = \frac{-\hbar^2}{2m} \partial_{xx} \Psi_j + g |\Psi_j|^2 \Psi_j + \epsilon_j \Psi_j - \nu (\Psi_{j-1} + \Psi_{j+1}), \quad (1)$$

where  $|\Psi_j(x, t)|^2 = n_j(x, t)$  represents the particle number density in each component. The linear coupling energy between neighboring condensates is  $\nu \geq 0$  and  $\epsilon_j$  is an energy bias that could, e.g., encode a trapping potential. For simplicity, we assume that the 1D inter-particle interaction strength  $g = 2\hbar\omega_{\perp}a$  is constant across the BEC array, where  $a$  is the  $s$ -wave scattering length and we have assumed that the 1D regime has been reached within a tight transverse trap of frequency  $\omega_{\perp}$ . In order to simplify the theoretical analysis and allow for closed-form analytical solutions, we assume the BECs to have infinite extent in  $x$  direction and consider a specific choice for the energy bias  $\epsilon_j$ :

- The *planar configuration* uses Dirichlet-type boundary conditions obtained by setting  $\Psi_0 \equiv 0 \equiv \Psi_{M+1}$  and an energy bias of

$$\epsilon_1 = \epsilon_M = -\nu \quad (2)$$

$$\epsilon_j = 0 \quad \text{for } 1 < j < M. \quad (3)$$

- The *ring configuration* uses periodic boundary conditions along the stack where  $\Psi_0 \equiv \Psi_M$  (and

$\Psi_1 \equiv \Psi_{M+1}$ ) with vanishing energy bias  $\epsilon_j = 0$ .

These conditions idealize the typical conditions that may be achieved in experiments simply for the purpose of finding simple closed-form solutions of the GPEs.

The stationary states  $\Psi_j(x, t) = \psi_j(x)e^{-i\mu t/\hbar}$ , with chemical potential  $\mu$ , satisfy the time-independent coupled GPEs

$$0 = \left( \frac{-\hbar^2}{2m} \partial_{xx} + g|\psi_j|^2 - \mu + \epsilon_j \right) \psi_j - \nu(\psi_{j-1} + \psi_{j+1}). \quad (4)$$

Stationary solutions corresponding to a constant density  $n$  in each component are found with  $\psi_j(x) = \sqrt{n} \exp(i\Phi)$  with  $gn = \mu + 2\nu > 0$  and arbitrary constant global phase  $\Phi$ .

For solitary waves solutions that only deviate locally from a constant background we define the solitary wave energy  $E_s$  as usual by

$$E_s = \int [(\epsilon_{\text{sol}} - \mu n_{\text{sol}}^{\text{tot}}) - (\epsilon_{\text{bg}} - \mu n_{\text{bg}}^{\text{tot}})] dx, \quad (5)$$

where  $\epsilon_{\text{sol}}$  and  $\epsilon_{\text{bg}}$  are the Gross-Pitaevskii energy densities of the solitary wave and background solutions, respectively, given by

$$\begin{aligned} \epsilon(x) = & \sum_{j=1}^M \frac{\hbar^2}{2m} |\partial_x \psi_j|^2 + \frac{g}{2} |\psi_j|^4 + \epsilon_j |\psi_j|^2 \\ & - \nu \psi_j^* (\psi_{j-1} + \psi_{j+1}), \end{aligned} \quad (6)$$

and the total particle number density is given by

$$n^{\text{tot}}(x) = \sum_{j=1}^M |\psi_j|^2. \quad (7)$$

The solitary wave solutions are localized and exponentially heal against the constant background, which is to be taken at the same chemical potential. Therefore, the integral in Eq. (5), which formally runs over an infinite domain, converges and in practice can be taken over a finite interval that is large compared to the localization length scale of the solitary wave. For the constant background, we find  $n_{\text{bg}}^{\text{tot}} = Mn$  and  $\epsilon_{\text{bg}} = Mgn^2/2 - 2M\nu n$ .

### B. Dark soliton stack

The stationary coupled GPEs (4) admit dark soliton solutions with identical wave functions in each BEC for both the planar and periodic configurations

$$\psi_j(x) = \sqrt{n} \tanh\left(\frac{x}{\xi}\right), \quad (8)$$

where  $n = (\mu + 2\nu)/g$  is the constant background density and the healing length  $\xi = \hbar/\sqrt{mg n}$  sets the relevant length scale for the soliton. The solution (8) represents

a kink in the wave function with a sign change at the identical position (here  $x = 0$ ) in all coupled condensates and completely aligned phases. We refer to the solution (8) as the *dark soliton stack*.

Note that the dark soliton stack solution (8) is independent of the linear coupling  $\nu$  when written in terms of the background density  $n$  and  $g$ . The solution has vanishing mass current density  $j_j(x)$  in each component, defined by

$$\begin{aligned} j_j(x) &= \frac{\hbar}{2im} (\Psi_j^* \partial_x \Psi_j - \Psi_j \partial_x \Psi_j^*) \\ &= n_j(x) \frac{\hbar}{m} \partial_x \arg \Psi_j, \end{aligned} \quad (9)$$

as well as vanishing Josephson current density  $j_{j,j+1}(x) \propto \arg \Psi_{j+1} - \arg \Psi_j$ . We symbolically denote the dark soliton stack with lined-up kinks in the BECs by  $\ast\ast\ast\ast$  for the case of  $M = 4$  BECs, as opposed to the node- and current-less background (ground-state) denoted by  $|||$ .

The energy of the dark soliton stack is  $E_s^{\text{DSS}} = ME_{\text{DS}}$ , where

$$E_{\text{DS}} = \frac{4}{3} \frac{\sqrt{gn}^{\frac{3}{2}} \hbar}{\sqrt{m}} \quad (10)$$

is the energy of a dark soliton in a single (scalar) one-dimensional BEC, as is easily verified from Eq. (5).

### C. Two coupled BECs

Let us first consider the case of  $M = 2$  coupled BECs, which has already been studied extensively [11, 18, 22]. Let us write the stationary coupled GPEs explicitly

$$\begin{aligned} 0 &= \left( \frac{-\hbar^2}{2m} \partial_{xx} + g|\psi_1|^2 - \tilde{\mu} \right) \psi_1 - \tilde{\nu} \psi_2, \\ 0 &= \left( \frac{-\hbar^2}{2m} \partial_{xx} + g|\psi_2|^2 - \tilde{\mu} \right) \psi_2 - \tilde{\nu} \psi_1. \end{aligned} \quad (11)$$

The planar and ring configuration become identical in this case of  $M = 2$  as the form (11) is obtained from the more general GPEs (4) in both the planar configuration, where  $\tilde{\nu} = \nu$  and  $\tilde{\mu} = \mu - \nu$ , and in the ring configuration, where  $\tilde{\nu} = \nu/2$  and  $\tilde{\mu} = \mu$ .

The constant density solutions with  $\tilde{\mu} + \tilde{\nu} = gn$  provide the background for the dark soliton stack (8), which exists for any value of  $\tilde{\nu} \geq 0$ . In addition, stationary *Josephson vortex* solutions exist when  $\tilde{\nu} \leq gn/4$  and take the form [11]

$$\begin{aligned} \psi_1^{(\otimes)}(x) &= \sqrt{n} \left[ \tanh\left(\frac{x}{\xi_{\tilde{\nu}}}\right) + i \sqrt{1 - \frac{4\tilde{\nu}}{gn}} \operatorname{sech}\left(\frac{x}{\xi_{\tilde{\nu}}}\right) \right], \\ \psi_2^{(\otimes)}(x) &= \left[ \psi_1^{(\otimes)}(x) \right]^*, \end{aligned} \quad (12)$$

where  $\xi_{\tilde{\nu}} = \hbar/\sqrt{4m\tilde{\nu}}$  is the  $\tilde{\nu}$ -dependent length scale of the Josephson vortex. The symbol  $\otimes$  denotes the clockwise orientation of currents of the Josephson vortex (positive in component  $\psi_1^{(\otimes)}$  and negative in  $\psi_2^{(\otimes)}$ ), symbolically represented as  $\uparrow \otimes \downarrow$ . A degenerate solution is the (*Josephson*) *anti-vortex*

$$\psi_i^{(\odot)} = \left[ \psi_i^{(\otimes)}(x) \right]^*, \quad (13)$$

for  $i = 1, 2$ , which has the opposite sense of rotation and is represented as  $\downarrow \odot \uparrow$ . In the following we will use the term Josephson vortex for both vortex  $\psi_i^{(\otimes)}$  and anti-vortex  $\psi_i^{(\odot)}$  solutions, unless the orientation matters. The solitary wave energy of the Josephson vortex (and the anti-vortex) evaluates to

$$E_s^{\text{JV}}(\tilde{\nu}) = 2\sqrt{\frac{\tilde{\nu}}{gn}} \left( 3 - 4\frac{\tilde{\nu}}{gn} \right) E_{\text{DS}}. \quad (14)$$

A linear stability analysis reveals that the dark soliton stack (for  $M = 2$ ) is dynamically stable in the regime where the Josephson vortex solutions do not exist ( $\tilde{\nu} > gn/4$ ) but dynamically unstable for  $0 < \tilde{\nu} < gn/4$ , where they are subject to decay into stable Josephson vortices [11, 18, 22]. In the absence of coherent coupling, at  $\tilde{\nu} = 0$ , and at  $\tilde{\nu} = gn/4$ , dark solitons are marginally stable, i.e. the frequency of the unstable mode vanishes. The critical value of the linear coupling  $\tilde{\nu} = gn/4$  (or, equivalently,  $\tilde{\nu}/\tilde{\mu} = \frac{1}{3}$ ) is further the location of a pitch-fork bifurcation where the Josephson vortex and anti-vortex solutions become identical to the dark soliton stack solution. This can be seen from the energy, since  $E_s^{\text{JV}}(gn/4) = 2E_{\text{DS}}$  and also directly from the wave function (12).

Another pitch-fork bifurcation takes place at  $\tilde{\nu}/\tilde{\mu} \approx 0.1413$  (or  $\tilde{\nu}/gn \approx 0.1238$ ) where two additional stationary solitary wave solutions split off from each of the Josephson vortex and anti-vortex solutions [22]. These asymmetric solutions were referred to as maxima of the Josephson vortex dispersion relation in Ref. [22]. Their essential character is revealed in the uncoupled limit ( $\nu \rightarrow 0$ ) where a dark soliton remains in only one of the components results. At finite coupling  $\nu > 0$  one BEC component has a stronger density depression and steeper phase gradients while the other component displays a backflow current, while generally the currents are weaker than in the Josephson vortex solutions. We represent such *half-dark-soliton* solutions schematically with  $\ast \downarrow$ , where the arrow indicates the orientation of the (weak) backflow current. Specifically, the vortex solution  $\uparrow \otimes \downarrow$  splits off two degenerate *half-dark-soliton* solutions with signatures  $\ast \downarrow$  and  $\uparrow \ast$ . The anti-vortex solution  $\downarrow \odot \uparrow$  analogously gives rise to half-dark-soliton solutions with signatures  $\ast \uparrow$  and  $\downarrow \ast$ . The half-dark-soliton solutions may be thought of being obtained by moving the vortex position from between the two BEC components onto one of them. They coexist with the stationary Josephson-vortex solutions (12) for  $\tilde{\nu}/\tilde{\mu} \lesssim 0.1413$ , have higher energy, but also different canonical momentum and phase

difference. The  $\tilde{\nu}$ -dependent energy  $E_s^{\text{JV}(M)}(\tilde{\nu})$  was computed in Ref. [22]. In the region where they exist, the stationary half-dark-solitons and Josephson vortices are all dynamically stable due to their position on the *grast* dispersion relation [22].

In the remainder of this paper we consider stationary solitary wave solutions for  $M > 2$  BECs.

#### D. Constructing solitary wave arrays from $M = 2$ solutions

The known solutions for  $M = 2$  coupled condensates can be used to generate solutions for larger arrays with  $M > 2$  for certain symmetric configurations. In particular the dark soliton stack as written in Eq. (8) is a solution of the coupled GPEs (4) for arbitrary  $M$  and for both the planar and ring configuration as defined in Sec. II A.

For an even number,  $M = 2r$ , of condensates, two types of solutions of Eqs. (4) can be constructed from known  $M = 2$  condensate solutions  $\psi_1 = A, \psi_2 = B$  defined by Eqs. (12):

1. *Flipped repetition*: The third and fourth component repeat components one and two in reverse order. The pattern can be extended for any even number of condensates.

$$(\psi_1, \psi_2, \psi_3, \dots, \psi_{2r}) = (A, B, B, A, A, B, \dots) \quad (15)$$

This solution is available for both the ring configuration and the planar configuration with  $\nu = \tilde{\nu}$  and  $\mu + \nu = \tilde{\mu}$ . The reason why this works is that each condensate in the elementary  $(A, B)$  unit is coupled to the nearest neighbor, which is identical. Therefore this linear coupling can be absorbed in adjusting the chemical potential  $\tilde{\mu}$  of the two-component equation (11).

2. *Alternating repetition*: The third and fourth component repeat components one and two in the same order. The pattern can be extended for any even number of condensates.

$$(\psi_1, \psi_2, \psi_3, \dots, \psi_{2r}) = (A, B, A, B, A, B, \dots) \quad (16)$$

This solution is only available for the ring configuration with  $2\nu = \tilde{\nu}$  and  $\mu = \tilde{\mu}$ . The reason why this works is that every condensate is coupled to two identical condensates, and thus the periodic  $M$ -condensate equation can be mapped onto the two-condensate GPE (11).

The solitary wave energy is additive for repeated configurations and thus one will obtain the  $r$ th multiple of the  $M = 2$  solitary wave energy. Let us specifically look at the possible solutions obtained for  $M = 4$ .

*Planar configuration of  $M = 4$  condensates.* Flipped repetition of the Josephson vortex (12) produces the configuration

$$a = \uparrow \otimes \downarrow \downarrow \odot \uparrow \quad (17)$$

with the explicit solution

$$\begin{aligned} \psi_1^{(a)}(x) &= \psi_4^{(a)}(x) = \psi_1^{(\otimes)}(x), \\ \psi_2^{(a)}(x) &= \psi_3^{(a)}(x) = \left[ \psi_1^{(\otimes)}(x) \right]^*, \end{aligned} \quad (18)$$

with  $\nu = \tilde{\nu}$  and  $\mu + \nu = \tilde{\mu}$ . Note that flipping the Josephson vortex in components 3 and 4 produces a Josephson anti-vortex. The energy of this configuration is

$$E_s^{(a)} = 2E_s^{\text{JV}}(\nu) = 4\sqrt{\frac{\nu}{gn}} \left( 3 - 4\frac{\nu}{gn} \right) E_{\text{DS}}. \quad (19)$$

A degenerate solution with reversed currents  $a^* = \downarrow \odot \uparrow \uparrow \otimes \downarrow$  is obtained by the complex conjugate of solution  $\psi_i^{(a)}$ .

The half-dark-soliton solutions of two-coupled condensate similarly produce solutions for  $M = 4$  condensates by flipped repetition. Four solutions can be constructed:

$$b_1 = * \downarrow \downarrow * \downarrow, \quad (20)$$

$$b_2 = \uparrow * * \uparrow, \quad (21)$$

$$b_3 = \downarrow * * \downarrow, \quad (22)$$

$$b_4 = * \uparrow \uparrow *. \quad (23)$$

These solutions are degenerate with energy  $E_s^{(b)} = 2E_s^{\text{JV}(M)}(\nu)$ .

*Ring configuration of  $M = 4$  condensates.* In ring configuration, periodic boundary conditions apply and additional coupling is possible between  $\psi_1$  and  $\psi_4$ . The same solutions  $a, a^*, b_i$  obtained for the planar configuration by flipped repetition are possible, since  $\psi_1 = \psi_4$  in these configurations. The solution  $a^*$  is depicted in Fig. 1. From each of the known solutions, we can construct one new (degenerate) solution by cyclic permutation  $\psi'_i = \psi_{i-1}$ , e.g.

$$a' = \uparrow \uparrow \otimes \downarrow \downarrow \odot, \quad (24)$$

where the last anti-clockwise vortex  $\odot$  connects component  $\psi_4$  with  $\psi_1$ .

Additional solutions can be constructed from alternating repetition. Applying this principle to the Josephson vortex solution (12), we obtain the solution

$$c = \uparrow \otimes \downarrow \odot \uparrow \otimes \downarrow \odot. \quad (25)$$

The explicit solution reads

$$\begin{aligned} \psi_1^{(c)}(x) &= \psi_3^{(c)}(x) = \psi_1^{(\otimes)}(x), \\ \psi_2^{(c)}(x) &= \psi_4^{(c)}(x) = \left[ \psi_1^{(\otimes)}(x) \right]^*, \end{aligned} \quad (26)$$

$2\nu = \tilde{\nu}$  and  $\mu = \tilde{\mu}$ . The energy is also given by twice the Josephson vortex energy, but now with a different interpretation of  $\tilde{\nu}$  in terms of the coherent coupling strength of the  $M = 4$  BEC array. We obtain

$$E_s^{(c)} = 2E_s^{\text{JV}}(2\nu) = 4\sqrt{\frac{2\nu}{gn}} \left( 3 - 8\frac{\nu}{gn} \right) E_{\text{DS}}. \quad (27)$$

Applying alternating repetition to the Josephson anti-vortex solution yields a degenerate configuration

$$c^* = \downarrow \odot \uparrow \otimes \downarrow \odot \uparrow \otimes, \quad (28)$$

which can alternatively be obtained by complex conjugation or cyclic permutation of  $c$ .

Alternating repetition of half-dark-soliton solutions yields another four degenerate configurations with energy  $E_s^{(d)} = 2E_s^{\text{JV}(M)}(2\nu)$ :

$$d_1 = * \downarrow * * \downarrow, \quad (29)$$

$$d_2 = \uparrow * \uparrow * \uparrow, \quad (30)$$

$$d_3 = \downarrow * \downarrow * \downarrow, \quad (31)$$

$$d_4 = * \uparrow * * \uparrow. \quad (32)$$

### E. Other solitary wave solutions

The solitary waves constructed in Sec. IID by flipped or alternating repetition do not exhaust the stationary solitary waves in the  $M$ -BEC array. In particular, the method described above does not allow us to construct solitary wave solutions in odd- $M$  arrays. But also for even  $M$ , the simplest non-trivial case being  $M = 4$ , there are inaccessible solutions. One example is the single Josephson vortex solution

$$\uparrow \uparrow \otimes \downarrow \downarrow, \quad (33)$$

which should exist as a stationary and stable solution in the planar configuration by analogy to the solitonic vortex solution known to exist in finite-width 2D and 3D waveguide geometries for BECs [32, 35, 37]. Other, less symmetric solitary waves consist as well and can be found by numerical procedures.

From a topological perspective, configurations like the solitonic vortex analog (33) with an unbalanced number of Josephson vortices cannot exist as finite- $E_s$  solitary waves in the ring configuration, where vortex lines that enter the ring also have to leave it. In the following section we will study the stability of solitary waves in the BEC array, which will also allow us to identify bifurcation points.

### III. LINEAR STABILITY OF THE DARK SOLITON STACK IN RING CONFIGURATION

In order to facilitate analytic results, we consider the ring configuration in the remainder of the paper. The

dark soliton stack (8) is a stationary solution of the coupled GPEs (1). In order to learn about its dynamical stability properties and bifurcation points we follow the well-know procedure of Refs. [30, 31, 35, 36] to linearize the time-dependent GPE (1) around the dark soliton solution (8) with the ansatz  $\Psi_j(x, t) = [\psi_j(x) + u_j(x)e^{-i\omega t} + v_j^*(x)e^{i\omega t}]e^{-i\mu t/\hbar}$ . We thus obtain the set of coupled Bogoliubov equations for the linear excitation modes with frequency  $\omega$  and amplitudes  $u_j(x), v_j(x)$  describing the small-amplitude excitations of the BEC  $\Psi_j$

$$\begin{aligned} H_j u_j + g n \tanh^2\left(\frac{x}{\xi}\right) v_j - \nu(u_{j-1} + u_{j+1}) &= \hbar\omega u_j \\ -H_j v_j - g n \tanh^2\left(\frac{x}{\xi}\right) u_j + \nu(v_{j-1} + v_{j+1}) &= \hbar\omega v_j, \end{aligned} \quad (34)$$

where  $H_j = -(\hbar^2/2m)\partial_{xx} + 2gn \tanh^2(x/\xi) - \mu$ .

Since the dark soliton solutions (8) are real-valued wave functions, it is convenient to re-arrange Eqs. (34) for the symmetric and antisymmetric combinations  $f_{j\pm} = u_j(x) \pm v_j(x)$ . In order to account for the  $j$  variation across the BEC array, we expand these modes in a plane wave basis along the  $j$ -direction (i.e. along the vertical direction in Fig. 1), that is

$$f_{j\pm}(x) = \sum_k f_{\pm}^{(k)}(x) e^{ik\xi y_j}, \quad (35)$$

where we have defined  $\xi_y = \sqrt{\hbar^2/2m\nu}$  as a length scale associated with the linear coupling  $\nu$ . We thus obtain

$$\left[ \frac{-\hbar^2}{2m} \partial_{xx} - g n \operatorname{sech}^2\left(\frac{x}{\xi}\right) + \lambda_k \right] f_{-}^{(k)} = \hbar\omega f_{+}^{(k)} \quad (36)$$

$$\left[ \frac{-\hbar^2}{2m} \partial_{xx} - 3g n \operatorname{sech}^2\left(\frac{x}{\xi}\right) + \lambda_k \right] f_{+}^{(k)} = \hbar\omega f_{-}^{(k)}, \quad (37)$$

where

$$\lambda_k = 2\nu [1 - \cos(k\xi_y)], \quad (38)$$

provides the dispersion relation along the  $j$  ‘‘coordinate’’, which can be seen as a synthetic second dimension (where we may consider  $y = j\xi_y$  a synthetic coordinate with the dimension of length). Because of the periodic arrangement of BECs, the wave number  $k$  can only take  $M$  values within the first Brillouin zone,

$$\frac{M\xi_y}{2\pi} k = 0, \pm 1, \pm 2, \dots, \frac{M}{2}, \quad (39)$$

and the transverse energy Eq. (38) represents a discrete spectrum.

The coupled Eqs. (36)–(37) [or equivalently Eqs. (34)] present a linear non-hermitian eigenvalue problem and thus permit, in principle, complex eigenvalues  $\omega$ . It is easy to see [e.g. by eliminating  $f_{+}^{(k)}$  from Eqs. (36)–(37)] that  $\omega^2$  is real-valued. Thus the possible solutions for  $\omega$

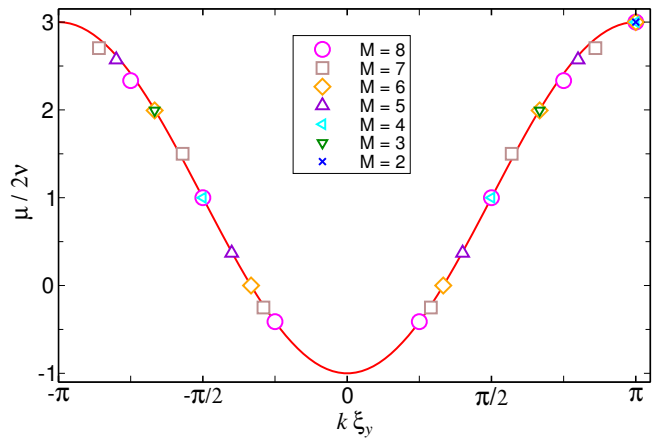


FIG. 2. Bifurcation points from the stationary dark solitons in systems with  $M = 2, \dots, 8$  linearly coupled BECs in a ring configuration. Transverse modes with discrete momentum  $k$  are excited along the effective dimension  $y$  introduced by the coherent coupling  $\nu$  (see text). The solid curve represents the analytical expression (41) and the open symbols correspond to the numerical solutions of Bogoliubov equations (34).

are either real, signifying stable normal modes, or purely imaginary, signifying dynamically unstable linear modes. At the transition between stable and unstable regions in parameter space, necessarily at least one normal mode frequency has to pass through zero. For this reason we solve Eqs. (36)–(37) for  $\omega = 0$  in order to obtain the stability boundaries.

In the absence of transverse excitations, i.e. for  $k = 0$  and then  $\lambda_k = 0$ , the Bogoliubov equations (36)–(37) have zero frequency modes (with  $\omega = 0$ ) that arise from the continuous symmetries of the system, the Goldstone modes. The Eqs. (36)–(37) furthermore decouple for  $\omega = 0$  and can be solved independently. Specifically, Eq. (36) is solved by  $f_{-}^{(0)} = \exp(i\theta)\sqrt{n} \tanh(x/\xi)$ , reflecting the symmetry of the stationary solution (8) against the selection of a global phase  $\theta$ . Equation (37) admits the Goldstone mode solution  $f_{+}^{(0)} = \xi \partial_x \sqrt{n} \tanh(x/\xi) = \sqrt{n} \operatorname{sech}^2(x/\xi)$ , which is localized at the density notch and corresponds to the invariance of Eq. (8) against translations along the axial coordinate.

In addition to the Goldstone modes, which arise from symmetries and thus are always present, the Bogoliubov equations (36)–(37) admit zero frequency ( $\omega = 0$ ) solutions under certain conditions, e.g. when normal modes become unstable, which is exactly where new nonlinear solutions bifurcate. We can find such solutions in the presence of transverse excitations, i.e. for  $k \neq 0$ . In particular, note that Eq. (36) with  $\omega = 0$  is a Schrödinger equation for  $f_{-}$  with a potential well defined by  $V(x) = -gn \operatorname{sech}^2(x/\xi)$ . The nodeless and localized (bound) ground state solution is known from the literature to take the form

$$f_{-}^{(k)}(x) = \sqrt{n} \operatorname{sech}\left(\frac{x}{\xi}\right), \quad (40)$$

with eigenvalue  $-gn/2$  [38]. This becomes a valid zero-frequency solution of the Bogoliubov equations, if the eigenvalue matches  $-\lambda_k$ , i.e.  $\lambda_k = gn/2 = (\mu + 2\nu)/2$ . Rewriting this equation as a condition relating the chemical potential and the linear coupling yields

$$\mu_b = 2\nu [1 - 2 \cos(k\xi_y)] . \quad (41)$$

This expression, which can be matched at the  $M-1$  discrete values  $k\xi_y = (\pm 1, \pm 2, \dots, M/2) \times 2\pi/M$ , indicates the existence of corresponding bifurcation points in the family of dark soliton states as a function of  $\mu$  (or equivalently, as a function of  $\nu$ ). Figure 2 shows a comparison of the analytical values given by Eq. (41) with the results obtained by numerically solving the Bogoliubov equations (34) for  $M = 2, \dots, 8$ . The tiny disagreement in the numerical values comes from a discretization error in the numerical data.

Solving the full Bogoliubov equations (34) numerically, reveals that the zero-frequency normal modes of Eq. (41) acquire imaginary frequency when  $\mu$  is increased (or  $\nu$  is decreased, respectively), signifying a dynamical instability of the dark soliton array. Figure 3 collects our numerical data for the unstable frequencies of dark solitons in different stacks ( $M = 2, 3, 4, 8$ ) with the same background density  $n = (\mu + 2\nu)/g$ . The vertical arrows under the horizontal axis point to the predicted bifurcations given by Eq. (41) and shown in Fig. 2. Now they are presented as a function of the linear coupling, after re-arranging Eq. (41):

$$\nu_b = \frac{gn}{4[1 - \cos(k\xi_y)]} . \quad (42)$$

For arrays with an even number of condensates  $M = 2, 4, 8$ , there are degenerate frequencies (and then also bifurcations) due to symmetries. Specifically, the same unstable modes present for  $M = 2$  reappear for  $M = 4$  where additional modes are present (and correspondingly for  $M = 8$ ). Due to the limited range of  $k$  values per Eq. (39), the relation between  $\nu_b$  and  $k$  is monotonic. Specifically, the unstable modes with larger  $k$  values are associated with a smaller critical coupling  $\nu_b$ . Since the instability regions overlap, the last critical coupling  $\nu_b$  that marks the region between stability and instability for the dark solitons occurs for the smallest modulus of  $|k| = 2\pi/M\xi_y$ . As a consequence, the dark soliton stack with overlapping dark solitons as per Eq. (8) is stable if

$$\frac{\nu}{gn} > \frac{1}{4[1 - \cos(2\pi/M)]} . \quad (43)$$

As we discuss in the next paragraph, this last instability threshold also marks the bifurcation of a single pair of Josephson vortex and Josephson antivortex from the dark soliton solution.

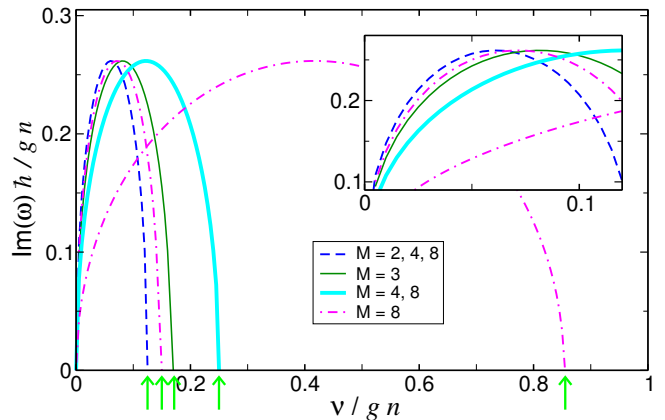


FIG. 3. Unstable excitation frequencies from the numerical solution of the Bogoliubov equations (34) for dark soliton states in stacks of  $M = 2, 3, 4, 8$  condensates in a ring configuration and varying coupling energy  $\nu$  [keeping the background density  $n = (\mu + 2\nu)/g$  constant]. The arrows under the horizontal axis indicate the bifurcation points (represented in Fig. 2), predicted by the analytical expressions (41) and (42).

#### IV. BIFURCATIONS OF JOSEPHSON VORTICES

The critical coupling values  $\nu_b$ , indicated by arrows in Fig. 3, mark the bifurcations of new families of solitary waves from the dark soliton stack (8) in the ring configuration. As described in Sec. IID, these families are made of stationary Josephson vortices that break the time reversal symmetry of the GPE (1) and present lower excitation energies than the original dark solitons. Figure 4 shows the energy of the two emerging branches (continuous lines) of solitary waves bifurcating from the  $M = 4$  dark-soliton stack (thick horizontal line). The bifurcations take place at values of the coupling parameter  $\nu_b = gn/4$  and  $\nu_b = gn/8$ , as obtained from Eq. (42) at the momentum values  $k\xi_y = \pm\pi$  and  $k\xi_y = \pm\pi/2$ . The states in these branches consist of, respectively, Josephson vortices in the configuration  $a = [\uparrow \otimes \downarrow \downarrow \odot \uparrow]$ , with energy given by Eq. (19), and the configuration  $c = [\uparrow \otimes \downarrow \odot \uparrow \otimes \downarrow \odot]$ , with higher energy than  $a$ , given by Eq. (27). As these solutions explicitly break the symmetry under reversal of current and with respect to cyclic permutation of the array (translation along the periodic array), such operations generate degenerate solutions, as previously discussed. This yields a total of four degenerate solutions of type  $a$  and two degenerate solutions of type  $c$ . Representative states are depicted in Fig. 5. In both cases the density profiles are equal for all the components. As the value of the coupling parameter  $\nu$  is increased, the density dips in the condensates deepen within each family. The same is also the case for the other states containing Josephson vortices.

For decreasing values of the coupling, the density-symmetric families of Josephson vortices  $a$  and  $c$  experience in turn additional bifurcations (discontinuous lines

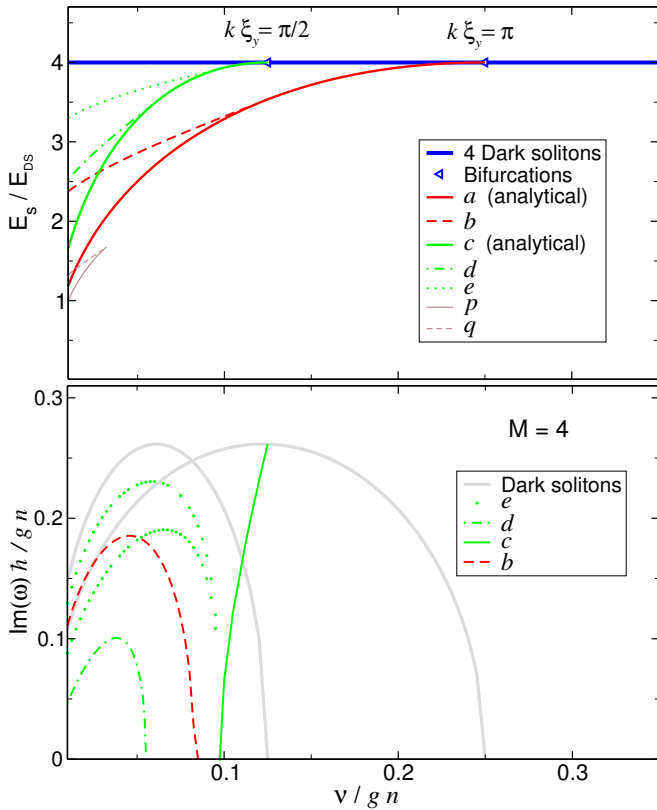


FIG. 4. Stationary solitary wave solutions in an array of  $M = 4$  BECs in ring configuration. Top panel: excitation energy vs. the linear coupling strength for solitary waves on the constant background density  $n = (\mu + 2\nu)/g$ . The dark soliton stack of Eq. (8) has constant energy with Josephson-vortex-type solutions bifurcating at the parameter values indicated with open triangles. The corresponding wave-number value from Eq. (42) (and Figs. 2 and 3) is indicated for each bifurcation point. See Figs. 5 and 6 for representative states in each branch. Bottom panel: unstable frequencies of the Bogoliubov spectrum of the solitary waves in the top panel. The configurations  $a$ ,  $p$  and  $q$  are always stable,  $d$ , and  $e$  always unstable, while configuration  $b$ ,  $c$ , and the dark soliton stack change stability in different regimes of  $\nu/gn$ .

in Fig. 4) that give rise to states with non equal density profiles along the stack. In particular, the half soliton states  $b = [* \downarrow \downarrow *]$  (dashed line) bifurcate from family  $a$ , whereas the half solitons  $d = [* \downarrow * \downarrow]$  (dash-dotted line) bifurcate from family  $c$ .

Besides, there are other stationary solutions in the 4-BEC stack that were not accounted for in Sec. IID. First, there is an additional bifurcation of family  $c$ , taking place at higher energy than branch  $d$ , which correspond to configurations of the type  $e = [* * * \downarrow]$  (dotted line in Fig. 4). When the linear coupling vanishes the energy of this branch equals  $3E_{DS}$ . Additionally, we have also found two branches of Josephson vortex type solutions that are disconnected from the families  $a$  to  $e$  presented before. They correspond to configurations of the type  $p = [\uparrow \uparrow \uparrow \otimes \downarrow \odot]$  (thin continuous line) and  $q = [\uparrow$

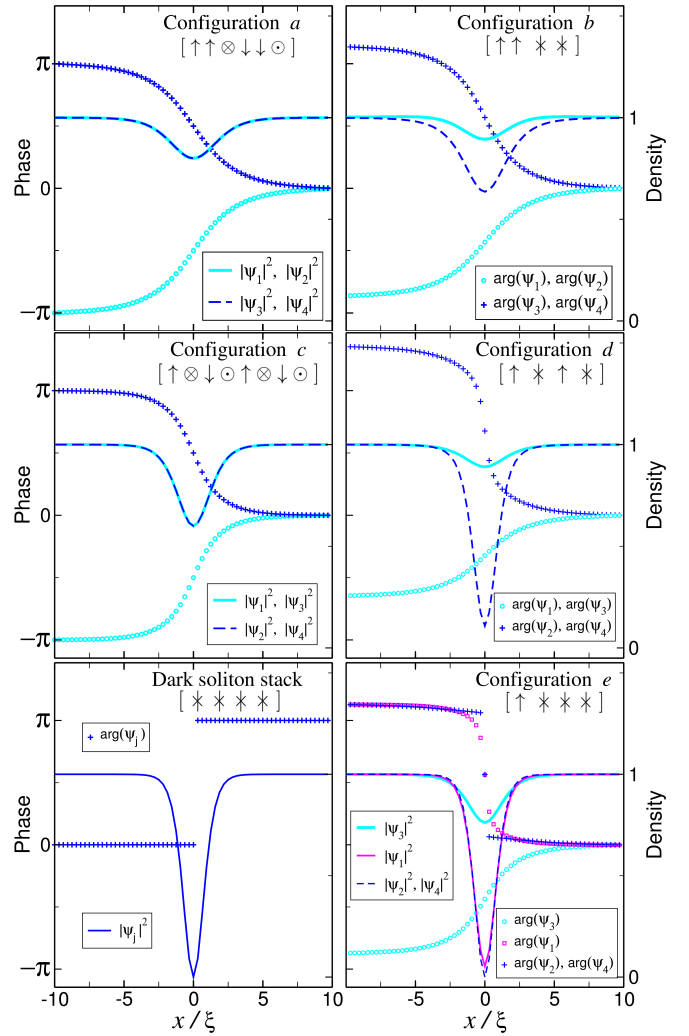


FIG. 5. Density and phase profiles of stationary solitary waves in a 4-BEC array in ring configuration with  $\nu = 0.05 gn$ : (symmetric) Josephson vortex solutions  $a$  and  $c$ , dark solitons, and fractional-dark-soliton configurations  $b$ ,  $d$  and  $e$ . Legends are shared between panels in the top and middle rows. Of the shown configurations only  $a$  and  $c$  are dynamically stable (see text). Density is reported in units of  $n$ .

$\uparrow \uparrow *]$  (thin dashed line), whose energies tend to zero and  $E_{DS}$ , respectively, when  $\nu \rightarrow 0$ . They merge at the maximum energy value, corresponding also to the maximum coupling value in both families.

In Fig. 5 we plot the density and the phase profiles of the solitonic states  $a$ - $e$  in the  $M = 4$  BEC array for the same value of the density and linear coupling  $\nu = 0.05 gn$ . For comparison, the dark soliton stack is also depicted in the bottom left panel. The profiles of configurations  $p$  and  $q$  are depicted in Fig. 6 for linear coupling  $\nu = 0.025 gn$ . As can be seen, these latter states, different from the other configurations, shape a density notch which does not extend to the whole array. In configuration  $p$ , a vortex dipole, made of a Josephson vortex and a Josephson antivortex, localizes around



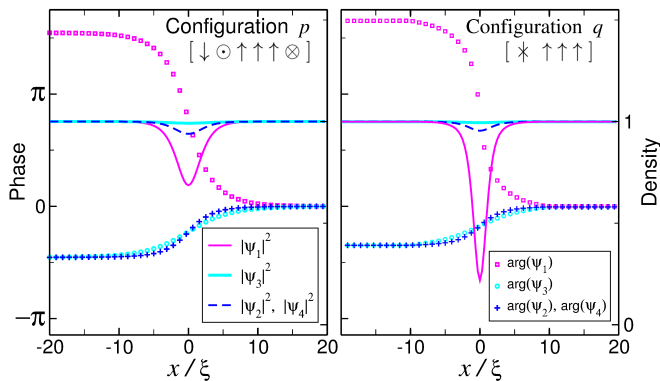


FIG. 6. Density and phase profiles of solitonic states  $p$  and  $q$  in an array of 4-BEC in ring configuration with  $\nu = 0.025 gn$ . Legends are shared by both panels. These states are dynamically stable. Density is reported in units of  $n$ .

a single strand. This solution is continuously connected to configuration  $q$ , which represents a solitary wave that is largely concentrated on a single strand. These solutions  $p$  and  $q$  represent solitary waves that are not only localized in  $x$  direction but along the transverse direction (i.e. along the array) and thus realize lump-type solitons. They very closely resemble the Jones-Roberts vortex-dipole and rarefaction-type solitary waves known in continuous two-dimensional BECs [39], with the difference that the latter always move with finite velocity whereas the solutions represented in Figs. 4 – 6 are stationary.

### A. Stability of bifurcating solitary waves

Regarding the stability, we have numerically solved the Bogoliubov equations for the linear excitations of the Josephson vortex solutions considered in Fig. 4. The frequencies of unstable excitations are plotted in the bottom panel of this figure. Among the states connecting with the dark soliton stack (through direct or secondary bifurcations) only the family with configuration  $a$ , the flipped configurations of Josephson vortices, contains dynamically stable states for all the values of the coupling parameter. The situation is more complicated for the other branches. The family of states with configuration  $c$  (alternating Josephson vortices) becomes only unstable from the point of the secondary bifurcation of branch  $e$  up to its junction with the dark soliton stack. The family  $b$  is also stable in a small range of couplings just before merging into its parent branch. Families  $d$  and  $e$  are always unstable. Interestingly, the two families  $p$  and  $q$ , disconnected from the dark soliton stack, contain dynamically stable states.

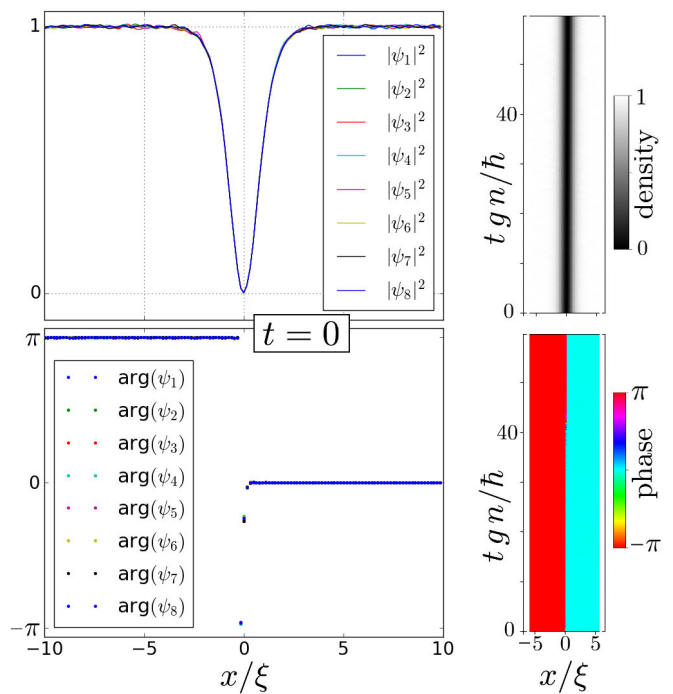


FIG. 7. Time evolution of a dark soliton stack with overlapping dark solitons in an array of  $M = 8$  BECs in ring configuration. The linear coupling parameter  $\nu/gn = 0.9$  is in the stable regime. Left panels: Initial density and phase profiles after a 1%-amplitude white-noise perturbation added to the wave function of Eq. (8). Right panels: Density (top) and phase (bottom) for one component (all components follow almost identical evolutions) are shown around the initial soliton position (at  $x = 0$ ) as a function of time (vertical axis). Density is reported in units of  $n$ .

### B. Real time evolution

In order to observe the dynamical emergence of Josephson vortices, we have performed numerical simulations of the time dependent GPE (1) for the real time evolution of overlapping dark solitons in the ring configuration. We have selected a study case with a stack of  $M = 8$  BECs and different values of the linear coupling parameter, so that the analytical predictions of the stable and unstable regimes of dark solitons can be checked. A white-noise perturbation, around 1% of the maximum amplitude, has been added to the initial stationary state, as shown in the two left panels of Fig. 7. Results from two series of simulations are reported here, namely for  $\nu/gn = 0.9$  in the stable regime of the dark soliton stack, shown in Fig. 7 (right panels), and  $\nu/gn = 0.14$  in the regime of multiple unstable modes, depicted in Fig. 8. The results confirm the predictions of the linear analysis summarized in Fig. 3.

In the stable case, the initial configuration survives to the initial weak perturbation. The right panels of Fig. 7 show the time evolution of the density and phase profiles, around the soliton position, up to  $t = 60 \hbar/gn$  for

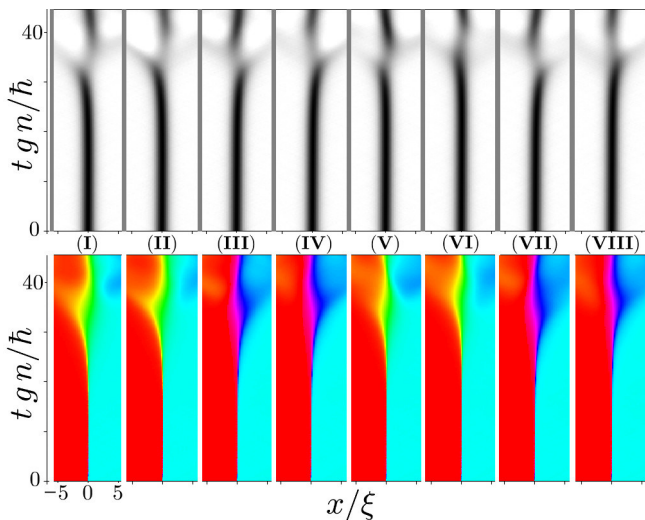


FIG. 8. Time evolution of an unstable dark soliton stack of  $M = 8$  BECs (identified by roman numerals) in a ring configuration with linear coupling  $\nu/gn = 0.14$  and the same initial conditions as in Fig. 7. Density (upper panels) and phase (lower panels) are shown around the initial soliton position (at  $x = 0$ ) as a function of time (vertical axis). The dark solitons' decay, consistent with the Bogoliubov analysis, is apparent after  $t = 20$ .

one of the components, the others being indistinguishable at the scale of the figure. The situation is quite different for the unstable case presented in Fig. 8, with  $\nu/gn = 0.14$ . In this case there are three pairs of unstable modes with momenta  $k\xi_y = (\pm 1, \pm 2, \pm 3) \times \pi/4$ , among which  $k\xi_y = \pm 2 \times \pi/4$  presents the maximum unstable frequency  $\omega \sim 0.25 gn/\hbar$  (see Fig. 3). It is therefore the latter mode that is expected to have the highest growth rate during the time evolution, and as a consequence, to cause the soliton decay. As can be seen in the graph, the expected decay starts between  $t = 15$  and  $20 \hbar/gn$ , a lifetime that depends on the type and amount of perturbation. A transient regime follows, between  $t = 30$  and  $40 \hbar/gn$ , characterized by wider density depletions and sound wave emissions. After this stage, the system reaches a configuration made of four Josephson vortices (the associated state bifurcated from the  $k\xi_y = \pm 2 \times \pi/4$  modes) in flipped repetition [  $\uparrow\uparrow \otimes \downarrow\downarrow \odot \uparrow\uparrow \otimes \downarrow\downarrow \odot$  ] that does not show further decay. Additionally we have checked that this state does not present imaginary frequencies in its Bogoliubov spectrum, thus it is dynamically stable.

## V. DISCUSSION AND CONCLUSIONS

In summary, we have shown that the array of linearly coupled BECs provides an excellent playground for the generation and manipulation of Josephson vortices and related solitary waves. Analytical and numerical evidence was presented for a rich landscape of dynam-

ically stable and unstable configurations. In particular the stable configurations should be accessible for experimental realization with optical lattices, where the lattice depth can control the linear coupling between 1D condensates [40, 41]. Multicomponent condensates with internal Josephson coupling (spinor condensates) could also realize a similar situation. The inter-component nonlinearities that are usually present in this case were not considered here and require further analysis along the lines of Ref. [22].

Our analysis of the instabilities and decay modes of the dark soliton stack reveals a close similarity to the snaking instability of dark soliton stripes in a continuous, confined superfluid [32, 36]. There, the system allows for quantized vibrations of the dark soliton plane according to the linear, normal modes of the transverse confinement. The nodal lines from the resulting standing waves translate into corresponding patterns of regular vortices after the soliton decay. When the transverse dimensions of the system are small compared to its axial length, the final stage of this decay leaves the simplest configuration, a solitonic vortex [32], which is dynamically stable. Analogously, in the dark soliton stack, the nodes of the standing wave perturbations across the dark soliton nodes in the BEC array correspond to the cores of the emerging Josephson vortices. While decay into a single Josephson vortex is possible in the planar configuration, the simplest situation in the BEC array in ring configuration is a (Josephson) vortex dipole, consisting of a Josephson vortex and a Josephson antivortex, which is dynamically stable. In addition, for small values of the linear coupling, we have also found dynamically stable states made of two Josephson dipoles that can be found at the final stage in the decay cascade of dark solitons.

The dark soliton stack of overlapping dark solitons across the array of BECs is found to be stable under the condition of the inequality (43), which is a condition on the parameters of nonlinearity  $gn$ , linear coupling  $\nu$ , and the number of BECs in the discrete array  $M$ . This gives a number of parameters that can be tuned to achieve stability, in particular the linear coupling  $\nu$ , which is controlled by the optical lattice. In contrast, the situation of a continuous BEC under trapping with frequency  $\omega$  reads  $\mu/\hbar\omega < 2.65$  [31, 36], which is not easily reached under typical experimental conditions [42–44].

These facts suggest a way for the experimental realization of stable dark solitons in optical lattices. Approximating the stability condition for the dark soliton stack (43) for a given number of components  $M \gg 1$  we obtain

$$\nu \gtrsim \frac{gn}{2} \left( \frac{M}{2\pi} \right)^2. \quad (44)$$

This condition can be experimentally realized for both the planar and the ring configuration with currently available optical trapping techniques. In the planar case one option is to combine a flat and elongated box potential [45] with a transverse optical lattice. The transverse size of the box defines the number of coupled BECs,

while the height of the optical lattice defines the tunneling coupling  $\nu$ . The interaction energy is adjustable by either tuning the density of the 1D gas or by exploiting a magnetic Feshbach resonance in order to change  $g$ . Another option is to populate selected 1D systems in a quantum gas microscope experiment [46, 47]. The special case of  $M = 2$  can be realized with help of atom chips [14]. The temperature should be chosen low enough to suppress strong thermal fluctuations in the 1D condensates [48]. Quantum fluctuations, which become relevant at low particle number densities, are not expected to destroy the soliton character but may lead to other effects like center-of-mass diffusion [49].

A ring shaped optical lattice as it is required for the ring configuration can be realized by interfering two Laguerre-Gaussian beams with different azimuthal quantum coordinates (i.e. topological charges)  $l_1$  and  $l_2$  and the same radial quantum coordinate  $p = 0$  such that only one ring is present in the intensity profile. The number of optical vortices where atoms can be trapped and thus the number of lattice sites is given by the difference in topological charge [50],  $M = |l_2 - l_1|$ . Laguerre-Gaussian beams can be created from Gaussian laser beams e.g. by

using spatial light modulators [50] or from circularly polarized light by a combination of an axially symmetric half wave plate and an axially symmetric polarizer [51].

Interesting future extensions of this work on standing waves in a 1D stack of BECs include the characterization of moving solitary waves and a multi-dimensional version where a 1D optical lattice slices a weakly trapped BEC into a stack of 2D pancakes. The results will be presented elsewhere.

## VI. ACKNOWLEDGEMENTS

CB acknowledges financial support by the DFG within the SFB/TR 49 and by the MAINZ graduate school. Furthermore, CB thanks Massey University for hospitality during a research visit where part of this work was completed. HO acknowledges financial support by the SFB/TR 185 "OSCAR". This work was supported by the Marsden Fund of New Zealand (Grant No. MAU1604).

- 
- [1] Paterno G Barone, A, *Physics And Applications Of The Josephson Effect* (Wiley, New York, 1982).
- [2] P. W. Anderson, "Considerations on the flow of superfluid helium," *Reviews of Modern Physics* **38**, 298–310 (1966).
- [3] B. M. Khorana, "ac josephson effect in superfluid helium," *Phys. Rev.* **185**, 299–308 (1969).
- [4] Emile Hoskinson, RE Packard, and Thomas M Haard, "Oscillatory motion: Quantum whistling in superfluid helium-4," *Nature* **433**, 376–376 (2005).
- [5] F Cataliotti, S. Burger, C Fort, P Maddaloni, F Minardi, A Trombettoni, A Smerzi, and M Inguscio, "Josephson Junction Arrays with Bose-Einstein Condensates," *Science* **293**, 843–846 (2001).
- [6] Michael Albiez, Rudolf Gati, Jonas Fölling, Stefan Hunsmann, Matteo Cristiani, and Markus K Oberthaler, "Direct observation of tunneling and nonlinear self-trapping in a single bosonic josephson junction," *Physical review letters* **95**, 010402 (2005).
- [7] S Levy, E Lahoud, I Shomroni, and J Steinhauer, "The ac and dc josephson effects in a bose-einstein condensate," *Nature* **449**, 579–583 (2007).
- [8] S Eckel, F Jendrzejewski, A Kumar, CJ Lobb, and GK Campbell, "Interferometric measurement of the current-phase relationship of a superfluid weak link," *Physical Review X* **4**, 031052 (2014).
- [9] Luigi Amico, Gerhard Birkel, Malcolm Boshier, and Leong-Chuan Kwek, "Focus on atomtronics-enabled quantum technologies," *New Journal of Physics* **19**, 020201 (2017).
- [10] Stefano Giovanazzi, Augusto Smerzi, and Stefano Fantoni, "Josephson effects in dilute bose-einstein condensates," *Physical review letters* **84**, 4521 (2000).
- [11] V. M. Kaurov and A. B. Kuklov, "Josephson vortex between two atomic Bose-Einstein condensates," *Physical Review A* **71**, 011601 (2005).
- [12] M. H. Devoret and R. J. Schoelkopf, "Superconducting circuits for quantum information: An outlook," *Science* **339**, 1169–1174 (2013).
- [13] Dimitri Roditchev, Christophe Brun, Lise Serrier-Garcia, Juan Carlos Cuevas, Vagner Henrique Loiola Bessa, Milorad Vlado Milošević, François Debontridder, Vasily Stolyarov, and Tristan Cren, "Direct observation of josephson vortex cores," *Nature Physics* **11**, 332–337 (2015).
- [14] Thomas Schweigler, Valentin Kasper, Sebastian Erne, Igor Mazets, Bernhard Rauer, Federica Cataldini, Tim Langen, Thomas Gasenzer, Jürgen Berges, and Jörg Schmiedmayer, "Experimental characterization of a quantum many-body system via higher-order correlations," *Nature* **545**, 323–326 (2017).
- [15] Shih-Wei Su, Shih-Chuan Gou, Ashton Bradley, Oleksandr Fialko, and Joachim Brand, "Kibble-Zurek Scaling and its Breakdown of Spontaneous Generation of Josephson Vortices in Bose-Einstein Condensates," *Phys. Rev. Lett.* **110**, 215302 (2013), arXiv:1302.3304.
- [16] V Kaurov and A Kuklov, "Atomic Josephson vortices," *Phys. Rev. A* **73**, 1–8 (2006).
- [17] J. Brand, T. J. Haigh, and U. Zülicke, "Rotational fluxons of Bose-Einstein condensates in coplanar double-ring traps," *Physical Review A* **80**, 011602 (2009).
- [18] Muhammad I Qadir, Hadi Susanto, and Paul C Matthews, "Fluxon analogues and dark solitons in linearly coupled bose-einstein condensates," *Journal of Physics B: Atomic, Molecular and Optical Physics* **45**, 035004 (2012).
- [19] D. Son and M. Stephanov, "Domain walls of relative phase in two-component Bose-Einstein condensates,"

- Phys. Rev. A* **65**, 063621 (2002).
- [20] Chunlei Qu, Marek Tylutki, Sandro Stringari, and Lev P. Pitaevskii, “Magnetic solitons in Rabi-coupled Bose-Einstein condensates,” *Phys. Rev. A* **95**, 033614 (2017), [arXiv:1609.08499](#).
- [21] Vladimir Gritsev, Anatoli Polkovnikov, and Eugene Demler, “Linear response theory for a pair of coupled one-dimensional condensates of interacting atoms,” *Phys. Rev. B* **75**, 174511 (2007).
- [22] Sophie S. Shamailov and Joachim Brand, “Quasiparticles of widely tuneable inertial mass: The dispersion relation of atomic Josephson vortices and related solitary waves,” *SciPost Phys.* **4**, 018 (2018), [arXiv:1709.00403](#).
- [23] Shih-Wei Su, Shih-Chuan Gou, I-Kang Liu, Ashton S Bradley, Oleksandr Fialko, and Joachim Brand, “Oscillons in coupled Bose-Einstein condensates,” *Phys. Rev. A* **91**, 023631 (2015), [arXiv:1412.5858](#).
- [24] T. W. A. Montgomery, W. Li, and T. M. Fromhold, “Spin Josephson Vortices in Two Tunnel-Coupled Spinor Bose Gases,” *Phys. Rev. Lett.* **111**, 105302 (2013), [arXiv:1211.6609](#).
- [25] A Gallemí, M Guilleumas, R Mayol, and A Muñoz Mateo, “Multidimensional Josephson vortices in spin-orbit-coupled Bose-Einstein condensates: Snake instability and decay through vortex dipoles,” *Physical Review A* **93**, 033618 (2016).
- [26] Richard A. Klemm, *Layered Superconductors* (Oxford University Press, 2011).
- [27] Yuri S Kivshar and Boris A. Malomed, “Dynamics of fluxons in a system of coupled Josephson junctions,” *Physical Review B* **37**, 9325–9330 (1988).
- [28] B. P. Anderson, P. C. Haljan, C. A. Regal, D. L. Feder, L. A. Collins, C. W. Clark, and E. A. Cornell, “Watching Dark Solitons Decay into Vortex Rings in a Bose-Einstein Condensate,” *Phys. Rev. Lett.* **86**, 2926–2929 (2001), [arXiv:0012444 \[cond-mat\]](#).
- [29] Mark J. H. Ku, Biswaroop Mukherjee, Tarik Yefsah, and Martin W Zwierlein, “Cascade of Solitonic Excitations in a Superfluid Fermi gas: From Planar Solitons to Vortex Rings and Lines,” *Phys. Rev. Lett.* **116**, 045304 (2016), [arXiv:1507.01047](#).
- [30] E. A. Kuznetsov and S. K. Turitsyn, “Instability and collapse of solitons in media with a defocusing nonlinearity,” *Sov. Phys. JETP* **67**, 1583–1588 (1988).
- [31] A. E. Muryshev, H. B. van Linden van den Heuvell, and G. V. Shlyapnikov, “Stability of standing matter waves in a trap,” *Phys. Rev. A* **60**, R2665–R2668 (1999).
- [32] Joachim Brand and William Reinhardt, “Solitonic vortices and the fundamental modes of the “snake instability”: Possibility of observation in the gaseous Bose-Einstein condensate,” *Phys. Rev. A* **65**, 043612 (2002).
- [33] A Cetoli, J Brand, R G Scott, F Dalfovo, and L P Pitaevskii, “Snake instability of dark solitons in fermionic superfluids,” *Phys. Rev. A* **88**, 043639 (2013), [arXiv:1307.3717](#).
- [34] S. Komineas and N. Papanicolaou, “Solitons, solitonic vortices, and vortex rings in a confined Bose-Einstein condensate,” *Phys. Rev. A* **68**, 043617 (2003).
- [35] A Muñoz Mateo and Joachim Brand, “Stability and dispersion relations of three-dimensional solitary waves in trapped Bose-Einstein condensates,” *New J. Phys.* **17**, 125013 (2015), [arXiv:1510.01465](#).
- [36] A. Muñoz Mateo and J. Brand, “Chladni Solitons and the Onset of the Snaking Instability for Dark Solitons in Confined Superfluids,” *Phys. Rev. Lett.* **113**, 255302 (2014), [arXiv:1408.0947](#).
- [37] L. A. Toikka and J. Brand, “Asymptotically solvable model for a solitonic vortex in a compressible superfluid,” *New J. Phys.* **19**, 023029 (2017), [arXiv:1608.08701](#).
- [38] N Rosen and Philip M Morse, “On the vibrations of polyatomic molecules,” *Phys. Rev.* **42**, 210 (1932).
- [39] C A Jones and P H Roberts, “Motions in a Bose condensate. IV. Axisymmetric solitary waves,” *J. Phys. A. Math. Gen.* **15**, 2599–2619 (1982).
- [40] MA Cazalilla, AF Ho, and Thierry Giamarchi, “Interacting bose gases in quasi-one-dimensional optical lattices,” *New Journal of Physics* **8**, 158 (2006).
- [41] Immanuel Bloch, Jean Dalibard, and Wilhelm Zwerger, “Many-body physics with ultracold gases,” *Reviews of modern physics* **80**, 885 (2008).
- [42] C. Becker, K. Sengstock, P. Schmelcher, P. G. Kevrekidis, and R Carretero-González, “Inelastic collisions of solitary waves in anisotropic Bose-Einstein condensates: slingshot events and expanding collision bubbles,” *New J. Phys.* **15**, 113028 (2013), [arXiv:1308.2994](#).
- [43] Mark J. H. Ku, Wenjie Ji, Biswaroop Mukherjee, Elmer Guardado-Sanchez, Lawrence W Cheuk, Tarik Yefsah, and Martin W Zwierlein, “Motion of a Solitonic Vortex in the BEC-BCS Crossover,” *Phys. Rev. Lett.* **113**, 065301 (2014), [arXiv:1402.7052](#).
- [44] Simone Donadello, Simone Serafini, Marek Tylutki, Lev P Pitaevskii, Franco Dalfovo, Giacomo Lamporesi, and Gabriele Ferrari, “Observation of Solitonic Vortices in Bose-Einstein Condensates,” *Phys. Rev. Lett.* **113**, 065302 (2014), [arXiv:1404.4237](#).
- [45] Alexander L. Gaunt, Tobias F. Schmidutz, Igor Gotlibovych, Robert P. Smith, and Zoran Hadzibabic, “Bose-Einstein Condensation of Atoms in a Uniform Potential,” *Phys. Rev. Lett.* **110**, 200406 (2013).
- [46] Jacob F. Sherson, Christof Weitenberg, Manuel Endres, Marc Cheneau, Immanuel Bloch, and Stefan Kuhr, “Single-atom-resolved fluorescence imaging of an atomic mott insulator,” *Nature* **467**, 68 (2010).
- [47] Christof Weitenberg, Manuel Endres, Jacob F. Sherson, Marc Cheneau, Peter Schau, Takeshi Fukuhara, Immanuel Bloch, and Stefan Kuhr, “Single-spin addressing in an atomic mott insulator,” *Nature* **471**, 319 (2011).
- [48] DS S Petrov, GV V Shlyapnikov, and JTM T M Walraven, “Regimes of Quantum Degeneracy in Trapped 1D Gases,” *Phys. Rev. Lett.* **85**, 3745–3749 (2000).
- [49] Sophie S. Shamailov and Joachim Brand, “Quantum dark solitons in the one-dimensional Bose gas,” (2018), [arXiv:1805.07856](#).
- [50] S. Franke-Arnold, J. Leach, M. J. Padgett, V. E. Lembessis, D. Ellinas, A. J. Wright, J. M. Girkin, P. Öhberg, and A. S. Arnold, “Optical ferris wheel for ultracold atoms,” *Opt. Express* **15**, 8619–8625 (2007).
- [51] Moritsugu Sakamoto, Kazuhiko Oka, Ryuji Morita, and Naoshi Murakami, “Stable and flexible ring-shaped optical-lattice generation by use of axially symmetric polarization elements,” *Opt. Lett.* **38**, 3661–3664 (2013).